

# Phage Langmuir-Blodgett Films for Biosensing Applications

Eric Olsen

Clinical Research Laboratory  
81<sup>st</sup> Medical Group  
Keesler AFB MS USA 39534  
eric.olsen@us.af.mil

Rajesh Guntupalli, Iryna Sorkulova, Robert Long,  
William Neely, Vitaly Vodyanov

Auburn University  
Auburn, AL USA 36849  
{guntura, sorokib, neelywc, ral0004, vodyavi}@auburn.edu

**Abstract**—The microstructure and functionality of methicillin-resistant *Staphylococcus aureus* (MRSA) biosensors prepared from novel Langmuir-Blodgett monolayers of lytic bacteriophage were characterized using scanning imaging ellipsometry (SIE) and scanning electron microscopy (SEM). SEM revealed uniform distribution of phage monolayers immobilized to biosensor substrates. SIE indicated monolayers were  $49.8 \pm 18.3$  nm thick on average. SIE charged couple imaging analysis of biosensors yielded an average intensity of  $159 \pm 7$  and  $194 \pm 13$  for  $10^8$  and  $10^9$  CFU/ml MRSA concentrations, respectively.

## I. INTRODUCTION

The ability to transfer homogeneous, well-controlled nanoscale Langmuir films of affinity bioreceptors from an air-water interface to a wide variety of substrates such as gold, mica and glass makes the Langmuir-Blodgett (LB) technique highly suitable for nanotechnology applications such as biosensors [1,2]. The functionality of bioreceptors as capture agents can be directly related to the experimental aspects of film preparation and transference; subphase pH, bioreceptor molecular orientation and spacing, and substrate properties [3,4] are all critical considerations. Thus, nanoscale characterization is an important consideration to understanding and optimizing self-assembly strategies for LB-based biosensors.

Scanning Imaging Ellipsometry (SIE) and Scanning Electron Microscopy (SEM) are two optical techniques that can help advance the design and fabrication of LB-based biological sensors. These methods afford non-invasive characterization of sufficiency and adequacy of transference of phage monolayers to substrates, including film thickness analysis, 3D mapping and monolayer surface imaging and visual examination, in comparison to other techniques such as atomic force microscopy, scanning tunneling microscopy, scanning force microscopy and x-ray diffraction. High-lateral resolution SIE promotes non-destructive quality control analysis during sensor fabrication and expedient biosensing using charged couple device (CCD) imaging or ellipsometry,

where changes in color intensity profile or thin-film thickness profile are proportional to the amount of bound target analyte, respectively.

We prepared and characterized stable, insoluble Langmuir films of methicillin-resistant *Staphylococcus aureus* (MRSA) bacteriophage by surface pressure-area ( $\Pi$ -A) isotherms then immobilized monolayer films by LB technique onto gold plated substrates to prepare MRSA biosensors and analyzed them by SEM and SIE.

## II. EXPERIMENTAL

### A. Biological and Chemical Components

Bacteriophage possessing lytic activity against type strain *S. aureus* (ATCC 12600) and other *S. aureus* strains was used as a bioreceptor for substrates [5,6]. 1,2-diphytanoyl-sn-glycero-3-phosphocholine ( $C_{48}H_{96}NO_8P$ ) (phospholipid) in chloroform (1 mg/ml) was obtained from Avanti Polar Lipids, Inc. (Alabaster, AL). Stearic acid ( $C_{18}H_{36}O_2$ ) powder (99% purity) was obtained from Alfa Aesar (Ward Hill, MA) and prepared as a solution (1 mg/ml) by dissolving into anhydrous hexane (Sigma Aldrich, St. Louis, MO).

### B. Substrates

Silica wafers (WaferNet Inc., San Jose, CA) were immersed in a piranha solution [ $3:1 NH_4OH:H_2O_2$ ] for 20 minutes at  $55^\circ C$  then rinsed in deionized water and air-dried [7]. Clean wafers were coated with a  $\sim 225$  nm thick gold layer over a  $\sim 50$  nm thick chromium adhesive interlayer using a Denton<sup>TM</sup> (Moorestown, NJ) high-vacuum RF sputter coater. The gold-plated substrates were cut into  $20 \text{ mm} \times 10 \text{ mm}$  strips and stored in a desiccator until use then rinsed in hexane prior to Langmuir film deposition.

### C. Surface Pressure-Area Isotherms and Langmuir Film Deposition to Substrates

The KSV 2200 LB film balance, experimental setup, and general procedures for preparing monolayers have been thoroughly described [8]. Stearic acid and phospholipid were

---

This research was performed and funded through United States Air Force (USAF) Clinical Investigations FDG20060049N and FKE20090002E, and USAF CRADA 07-277-60MDG-01. Auburn University Detection and Food Safety Center fund also supported this work in part.

used as standards for isotherm analysis in comparison to phage. Phage monolayers were formed by spreading 200  $\mu\text{l}$  phage ( $2.94 \times 10^{12}$  plaque forming units/ml) in suspension onto the subphase via a partially immersed glass rod. Similarly, phospholipid monolayers were prepared with 30  $\mu\text{l}$  of phospholipid suspension and stearic acid monolayers were prepared with 20  $\mu\text{l}$  of stearic acid suspension. The film was equilibrated for 20 minutes then isotherm analysis was conducted by compressing the monolayer over the defined area of the trough at constant rate (30 mm/min) and temperature ( $30 \text{ mm/min}$ ,  $20 \pm 0.1^\circ\text{C}$ ) while surface pressure measurements were recorded. Isotherms of each material (phage, phospholipid or stearic acid) provided the optimal pressure in mN/m for deposition to substrates.

Optical biosensors were prepared by compressing phage, phospholipid or stearic acid films to optimally determined surface pressures of 18, 17 and 47 mN/m, respectively, then vertically dipping clean substrates up and down through the film monolayer at a rate of 4.5 mm/min [9].

#### D. Monolayer and Biosensor Characterization

LB monolayers on substrates were evaluated with a JEOL-7000F SEM (JEOL USA Inc., Peabody, MA). Samples were air-dried at ambient temperature then mounted onto aluminum stubs with copper adhesive tape (Ted Pella Inc., Redding, CA) and sputter-coated. Micrographs were taken using an accelerating voltage of 5 kV and probe current of 54  $\mu\text{A}$ . Images were captured electronically using JEOL-Imaging software. No biological staining agents were utilized.

LB monolayers on substrates were also analyzed using an auto-nulling SIE (EP<sup>3</sup>, Nanofilm Technologies, Göttingen, Germany) (Fig. 1a). Thickness measurements were taken in PCSA (Polarizer, Compensator, Sample, Analyzer) configuration: solid state laser source ( $\lambda = 532 \text{ nm}$ ), a xenon arc lamp with 46 interference filters ( $\lambda = 300 \text{ to } 1000 \text{ nm}$ ), and  $10\times$  objective with  $2 \mu\text{m}$  spatial resolution and  $60^\circ$  angle of incidence to the substrate surface's perpendicular axis. All measurements were taken at room temperature ( $25 \pm 2^\circ\text{C}$ ) using air as the ambient medium.

Computerized optical modeling software (EP<sup>3</sup> View) allowed analysis of thickness and refractive index data for immobilized monolayers on substrates (Fig. 1b). Estimated values were assigned to unknown parameters (such as layer thickness) for the purpose of preliminary calculations. These free parameters were varied until a minimum mean squared error was achieved, which was used to verify the consistency of measured and simulated data.

An ellipsometric null condition was induced by detecting minimum intensity at the CCD camera while changing P, C and A component settings. Component angles of P, C and A settings at the null condition were determined by the thin film's optical properties. Biosensors were evaluated using the SIE's CCD camera capability.

Quantitative phage deposition studies were verified using a Quartz Crystal Microbalance (QCM) [10].

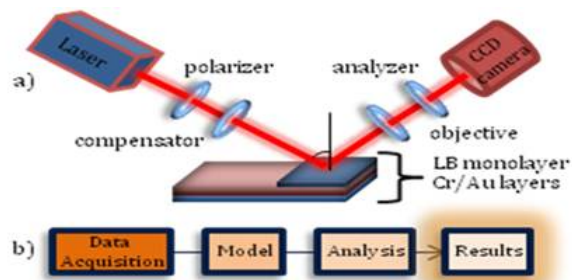


Fig. 1. (a) Schematic of spectroscopic imaging ellipsometer and (b) flow chart for data analysis.

### III. RESULTS AND DISCUSSION

#### A. Monolayer Isotherms

Stable Langmuir films of *S. aureus*-specific lytic phage, phospholipid or stearic acid were prepared at an air-water interface. Isotherms were measured by gradually compressing the prepared surface monolayer film at constant rate and temperature into a defined area (LB trough) while monitoring changes in surface pressure. The stearic acid monolayer (Fig. 2a-1) exhibited a moderate gaseous phase of  $<2 \text{ mN/m}$ , requiring only 25% of compression before reaching a liquid-expanded state. The phospholipid monolayer (Fig. 2a-2) also exhibited a very short gaseous phase of  $<2 \text{ mN/m}$ , requiring about 10% compression. These isotherm results principally agree with the literature [11-13] although the stearic acid's monolayer zero pressure (Table 1) was slightly larger than that of published results [14] and was attributed to subphase composition. The phage monolayer (Fig. 2b) was characterized by a long gaseous phase of  $<10 \text{ mN/m}$ , requiring about 60% compression before a liquid-expanded state was reached, and exhibited a shoulder at  $\sim 7 \times 10^4 \text{ nm}^2/\text{phage}$  particles.

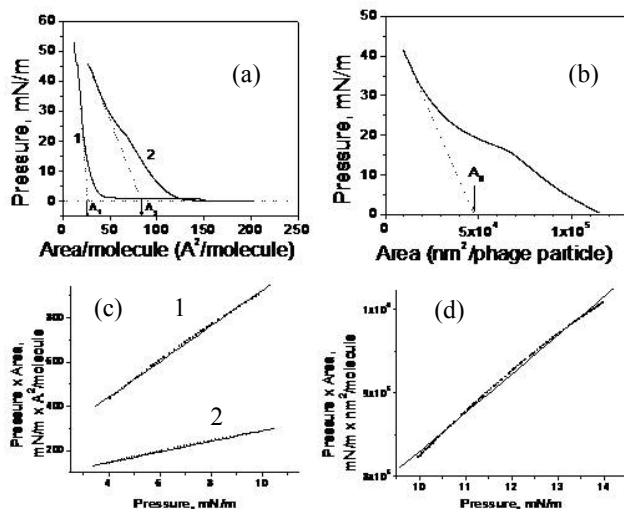


Fig 2.  $\Pi$ -A isotherms: (a) stearic acid (1) and phospholipid (2). The estimated zero-pressure areas for stearic acid and phospholipid ( $A_1$  and  $A_2$ ) were equal to  $23 \pm 1.0$  and  $81 \pm 2 \text{ Å}^2/\text{molecule}$ , respectively. (b) Phage monolayer. The estimated zero-pressure area for phage ( $A_0$ ) was  $47 \pm 2 \times 10^3 \text{ nm}^2/\text{phage particle}$ . Volmer presentation of isotherms: (c) stearic acid (1) and phospholipid (2). Points are experimental data, lines are linear

regressions (1:  $R = 0.999$ ,  $p < 0.0001$ , slope =  $24.1 \pm 0.2 \text{ \AA}^2/\text{molecule}$ ; 2:  $R = 0.999$ ,  $p < 0.0001$ , slope =  $80.6 \pm 0.4 \text{ \AA}^2/\text{molecule}$ ). (d) phage monolayer.

Points are experimental data, line is a linear regression (1:  $R = 0.998$ ,  $p < 0.0001$ , slope =  $46.4 \pm 0.26 \times 10^3 \text{ nm}^2/\text{molecule}$ ).

The specific areas were estimated by extrapolating “zero-pressure” areas [14] and a two-dimensional modification of the van der Waals equation of state [15-17]:

$$(\Pi + a/A^2)(A - A_e) = kT \quad (1)$$

where  $A$  represents a specific molecular area,  $a$  is intermolecular interaction term,  $A_e$  is an excluded specific area,  $k$  is the Boltzmann constant,  $\Pi$  is the surface pressure, and  $T$  is the absolute temperature. At small interactions and large specific areas, (1) can be reformed as a Volmer-type equation [18-20]:

$$\Pi A = kT + A_e \Pi \quad (2)$$

Equation (2) can be represented as a linear plot of the left-side expression versus the surface pressure and yields an estimate of  $A_e$ . The excluded area is derived from the slope of the line and represents the area around a single phage inaccessible to other phage due to structural hindrances.

Calculated excluded molecular areas for stearic acid ( $24.1 \pm 0.2 \text{ \AA}^2/\text{molecule}$ ), phospholipid ( $80.6 \pm 0.4 \text{ \AA}^2/\text{molecule}$ ) (Fig. 2c) and phage monolayers  $46.4 \pm 0.26 \times 10^3 \text{ nm}^2/\text{molecule}$  (Fig. 2d) concur well with observed zero pressure data from isotherms and literature (Table I), indicating that when lytic phage was deposited to the water-air interface, a stable monolayer film was formed. A single phage capsid volume is  $\sim 6000$  times larger than that of a phospholipid molecule yet the phage monolayer produced a stable, reproducible isotherm that withstood surface pressures up to  $\sim 40 \text{ mN/m}$ . This is both novel and unexpected.

$\Pi$ - $A$  isotherm data was further analyzed to determine the compressibility modulus (elasticity) of films, which describes compactness and film stability (Fig. 3). Taken together, isotherm and elasticity analysis indicated that constant surface pressures of 18, 17, and 47  $\text{mN/m}$  were optimal for transference of phage, phospholipid and stearic acid, respectively, to substrates.

TABLE I. MOLECULAR AREA OF MONOLAYERS

Monolayer	Zero pressure area	Excluded area	Literature data
Stearic acid	$23 \pm 1.0 \text{ \AA}^2/\text{molecule}$	$24.1 \pm 0.2 \text{ \AA}^2/\text{molecule}$	$21 \text{ \AA}^2/\text{molecule}$ [10,11]
Phospholipid	$81 \pm 2 \text{ \AA}^2/\text{molecule}$	$80.6 \pm 0.4 \text{ \AA}^2/\text{molecule}$	$81 \text{ \AA}^2/\text{molecule}$ [12]
Phage	$4.7 \pm 0.2 \times 10^4 \text{ nm}^2/\text{phage particle}$	$4.6 \pm 0.26 \times 10^4 \text{ nm}^2/\text{phage particle}$	Not available

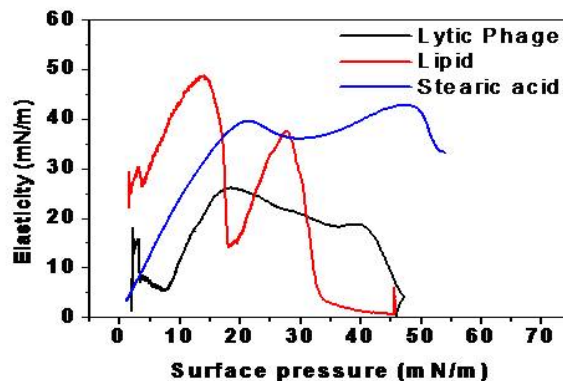


Fig. 3. Elasticity of lytic phage, lipid and stearic acid monolayers as a function of surface pressure at  $20 \pm 0.1^\circ\text{C}$ .

### B. Modeling of Phage at the Air-Water Interface

Isotherm analysis yields insights to phage positioning at the air-water interface under differing conditions of pressure (Fig. 4). At low concentrations, phage are widely-spaced and behave as a gaseous phase and most likely assume a horizontal orientation similar to that of tobacco mosaic virus particles [21,22]. However, as the film is compressed, phage become densely packed and space is reduced at the plane of the air-water interface, resulting in many reorienting to an inclined or strictly vertical position, capsid-down and tail-up. Phage tail orientation in the film is critical since it is responsible for capturing the target (MRSA) in the virus’s natural infective process.

At the liquid expanded phase, the monolayer consists of a mixture of horizontal and inclined phages, which coincides with the shoulder observed in the  $\Pi$ - $A$  isotherm (Fig 2b). Similar shoulders have been observed in other monolayers near the liquid-expanded/liquid-condensed phase transition at the air-water interface. It has been shown that this transition is accompanied by a reorientation of the molecules and that the different phases are separated by an inhomogeneous coexistence region on the isotherms [23,24].

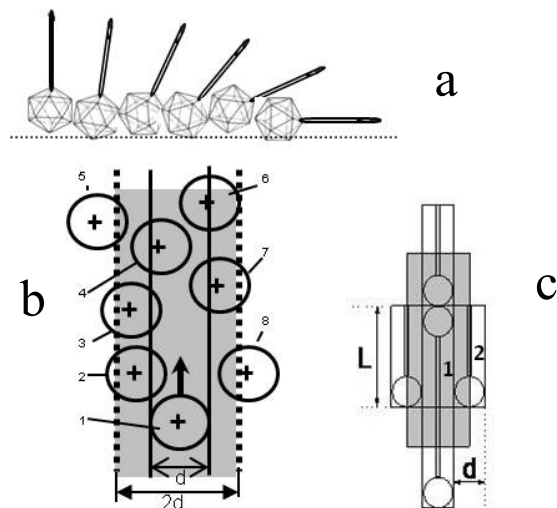


Fig. 4. Packing models of phage on the water/air interface. (a) One dimensional model of phage assuming that phages can change orientation from horizontal to oblique, and to vertical as surface pressure change from small to high (from right to left). (b) The sketch for excluded area of phage in vertical orientation. The phage heads are approximated by discs with diameter,  $d$ . The phage, 1, occupies an area  $A = \pi d^2/4$ . The excluded area is estimated by an area of interacted phage. When phage 1 is moving in direction indicated by an arrow, it will collide with phage (2, 3, 4, 6, and 7) whose centers (+) are inside the  $2d$  diameter circle. The excluded area (shaded region in Figs. 4b and 4c) equals  $\pi d^2$ . Two phage in close proximity can share the excluded area; therefore, the excluded area per phage equals half of the inaccessible area ( $\pi d^2/2$ ). (c) The sketch for excluded area of phage in horizontal orientation. The central phage, 1, occupies area  $A = Ld$ , where  $L$  is a length of a whole phage.

### C. SEM

SEM revealed nearly homogenous phospholipid (Fig. 5a) and stearic acid (Fig. 5b-1) monolayers on substrates with no visible discontinuities. In comparison, phage (Fig. 5c) had an estimated average ( $n = 10$ ) adsorption of  $8.84 \pm 0.6$  phage per square micron on substrates. This correlated well with quantitative QCM studies (Fig. 6) that showed an adsorption of 9.6 phage per square micron on gold plated resonators. Monolayers appeared as patches covering  $\sim 10\%$  of substrates on average. The LB method increased substrate surface coverage 100% in comparison to phage immobilization through biotinylation [25]. The LB method is much more effective and efficient than simple physical adsorption (Fig. 5d) for immobilizing phage in the correct orientation to substrates [10].

SEM analysis indicated that phage possessed slightly oval heads measuring  $90 \pm 6 \text{ nm} \times 108 \pm 7 \text{ (SE) nm}$  and tails measuring  $196 \pm 8 \text{ (SE) nm}$  in length and  $21 \pm 1 \text{ (SE) nm}$  in diameter. The cross-sectional area of a phage through the middle of head and tail was equal to  $\sim 1.2 \times 10^4 \text{ nm}^2$ . These dimensions agree well with those found for staphylococcal phage [26-28]. The average thickness of phage monolayer estimated from micrographs was equal to  $39.0 \pm 8.0 \text{ nm}$ .

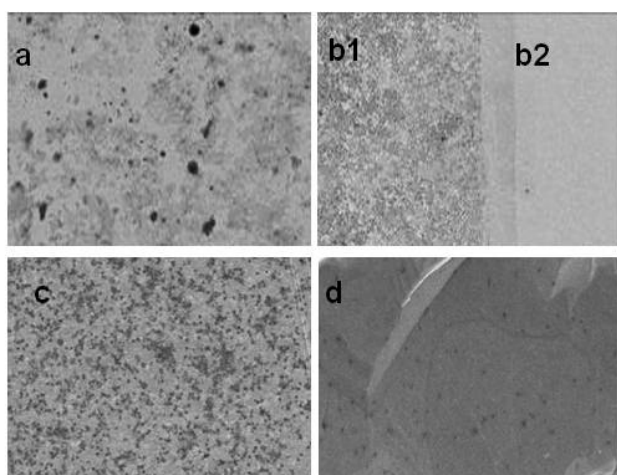


Fig. 5: SEM micrographs of a) phospholipid, b1) stearic acid and c) phage deposited to substrates by LB method in comparison to b2) clean substrate devoid of monolayer and (d) phage adsorbed to substrate by physical adsorption.

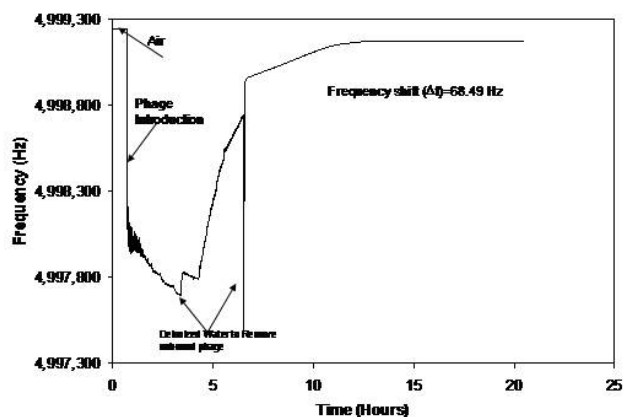


Fig. 6. Representative QCM graph depicting frequency change as a function of phage adsorption to gold-plated resonator over time. Application of phage in suspension to a clean, dry resonator at steady state:  $4,999,242 \pm 0.5 \text{ Hz}$ .

Unbound phage were removed by gently washing with deionized water followed by air-drying of resonator. Dried resonator with adsorbed phage at steady state:  $4,999,174 \pm 0.5 \text{ Hz}$ . Frequency shift caused by phage ( $\Delta f$ ) =  $-68 \pm 0.5 \text{ Hz}$ , which equates to frequency shift caused by  $1.21 \times 10^9$  bound phage particles or 9.6 phage per square micron.

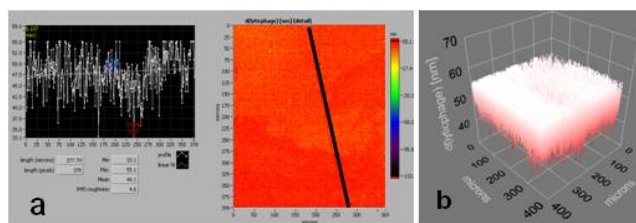


Fig. 7. (a) and (b) are an ellipsometric thickness profile and 3D thickness map of a lytic phage, respectively (effective refractive index = 1.05). Thickness profiles show mean, RMS roughness, minimum, and maximum thickness of the monolayer. The line across the thickness map was drawn to generate the thickness profile

### D. SIE

3-D thickness profiles from delta mapped SIE images revealed average monolayer thicknesses of  $49.8 \pm 18.3 \text{ nm}$ ,  $21.4 \pm 2.1 \text{ A}^\circ$  and  $18.5 \pm 1.6 \text{ A}^\circ$  for phage (Fig. 7), phospholipid and stearic acid, respectively. Surface substrate profiles showed phospholipid and stearic acid monolayers oriented at  $38.9 \pm 2.1^\circ$  and  $40.3 \pm 4.1^\circ$  angles, respectively.

### E. SIE-based biosensor for MRSA

Formation of a thin film due to bioreceptor (phage)-target (MRSA) interaction at the sensor surface altered the interference pattern of light and was analyzed by SIE either through the charge-coupled device (CCD) imaging (measuring color intensity differences) or ellipsometry (measuring thin film thickness). The changes in intensity profile or thickness profile was proportional to the amount of bound target analyte. Preliminary SIE CCD imaging analysis of post-assayed MRSA-phage substrate yielded an average relative intensity (arbitrary units) of  $159 \pm 7$  (Fig. 8a) and  $194 \pm 13$  (Fig. 8b) for MRSA concentrations of  $10^8$  and  $10^9 \text{ CFU/ml}$ , respectively. Visible differences in the bacterial coverage can also be seen in Figs. (8a and 8b-left) due to cell distribution as well as the

intensity profile with varying concentrations of MRSA. After optimizing each step the total assay time could be reduced to less than 10 minutes.

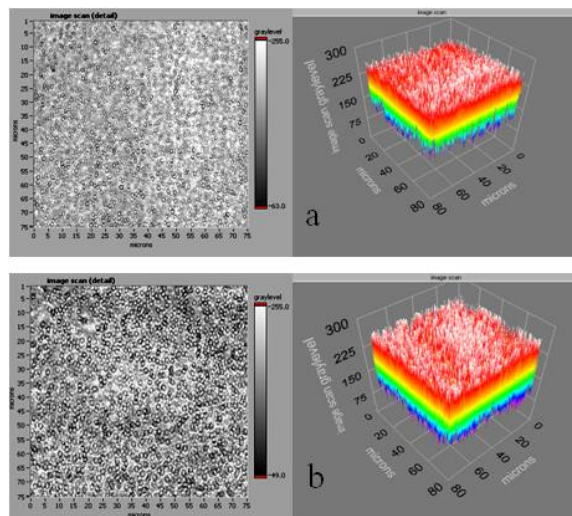


Fig. 8: Representative CCD camera image and 3D intensity profile of MRSA at concentrations of (a)  $10^8$  CFU/ml, and (b)  $10^9$  CFU/ml attached to phage bioreceptors immobilized on glass substrates.

#### IV. CONCLUSION

We demonstrated that stable, insoluble Langmuir monolayers could be formed at an air-water interface using lytic bacteriophage. The phage gradually orient themselves from a horizontal position parallel to the air-water interface to a vertical position with phage capsids immersed into the interface as surface pressure increases. Surface pressure-area dependence was found to be described well by the Volmer equation of state for horizontal orientation to the air-water interface at low surface pressures. Phage specific adsorption in Langmuir monolayers transferred to substrates and measured by SEM is consistent with that calculated independently from  $\Pi$ -A isotherms at the transfer surface pressure of 18 mN/m. Lytic phage, phospholipid and stearic acid monolayers were transferred onto solid gold coated substrates using the LB technique. These monolayers were characterized for quality and thickness with SEM and SIE. SEM showed phage monolayers occupying approximately 10% of substrate, where as stearic acid and phospholipid monolayers showed nearly 100% of area coverage of substrates. Prepared sensors were capable of binding MRSA at  $10^8$  -  $10^9$  CFU.ml.

We conclude that SIE measurement and SEM micrographs have potential use in quality control measures when LB films are used in the preparation of nanotech devices such as biosensors for the detection of pathogenic bacteria.

#### ACKNOWLEDGMENT

The views expressed in this article are those of the authors, and do not reflect the official policy or position of the United States Air Force, Department of Defense, or the U.S. Government.

#### REFERENCES

- [1] R. Guntupalli, et al., "Rapid and sensitive magnetoelastic biosensors for the detection of *Salmonella* Typhimurium in a mixed microbial population," *J. Microbiol. Methods*, pp. 112-118, 2007.
- [2] R. Guntupalli, et al., "A magnetoelastic resonance biosensor immobilized with polyclonal antibody for the detection of *Salmonella* Typhimurium," *Biosens. Bioelectron.*, pp. 1474-1479, 2007.
- [3] A.H.R. Flood, et al., "Meccano on the nanoscale-a blueprint for making some of the world's tiniest machines," *Aust. J. Chem.*, pp. 301-322, 2004.
- [4] D.R. Talham, "Conducting and magnetic Langmuir-Blodgett films," *Chem. Rev.*, pp. 5479-5501, 2004.
- [5] S. Balasubramanian, I.B. Sorokulova, V.J. Vodyanoy, and A.L. Simonian, "Lytic phage as a specific and selective probe for detection of *Staphylococcus aureus* - a surface plasmon resonance spectroscopic study," *Biosens. Bioelectron.*, pp. 948-955, 2007.
- [6] R. Guntupalli, et al., "Real-time optical detection of methicillin-resistant *Staphylococcus aureus* using lytic phage probes," *Biosens. Bioelectron.*, pp. 151-154, 2008.
- [7] R. White, "Piranha clean," [http://engineering.tufts.edu/microfab/index\\_files/SOP/PiranhaClean\\_SOP.pdf](http://engineering.tufts.edu/microfab/index_files/SOP/PiranhaClean_SOP.pdf), available on-line.
- [8] E.V. Olsen, et al., "Specific and selective biosensor for *Salmonella* and its detection in the environment," *J. Microbiol. Methods*, pp. 273-285, 2003.
- [9] S.T. Pathirana, et al., "Rapid and sensitive biosensor for *Salmonella*," *Biosens. Bioelectron.*, pp. 135-141, 2000.
- [10] E. Olsen, A. Vainrub, and V. Vodyanoy, "Acoustic Wave (TSM) Biosensors: Weighing Bacteria," in *Principles of Bacterial Detection: Biosensors, Recognition Receptors and Microsystems*, M. Zourob, S. Elwary, and A. Turner, Eds. New York: Springer, 2008, pp 252-298.
- [11] M.N. Islam, D. Bhattacharjee, and S.A. Hussain, "Monolayer characteristics of pyrene mixed with stearic acid at the air-water interface," *Surf. Rev. Lett.*, pp. 287-293, 2008
- [12] S. Pathirana, W.C. Neely, L.J. Myers, and V. Vodyanoy, "Interaction of valinomycin and stearic acid in monolayers," *Langmuir*, pp. 1984-1987, 1992
- [13] H. Hussain, A. Kerth, A. Blume, and J. Kressler, "Amphiphilic block copolymers of poly(ethylene oxide) and poly(perfluorohexylethyl methacrylate) at the water surface and their penetration into the lipid monolayer," *J. Phys. Chem. B*, pp. 9962-9969, 2004.
- [14] G.L. Gaines, *Insoluble Monolayers at Liquid-Gas Interfaces*. Interscience: New York, 1966.
- [15] A.K. Rakshit, G. Zografu, I.M. Jalal, and F.D. Gunstone, "Monolayer properties of fatty acids: II, surface vapor pressure. *J. Colloid and Interface Sci.*, pp. 466-473, 1981.
- [16] J.C. Sykora, W.C. Neely, and V. Vodyanoy, "Thermodynamic characteristics of mixed monolayers of amphotericin B and cholesterol," *J. Colloid and Interface Sci.*, pp. 60-67, 2004.
- [17] P. Dynarowicz-Latka, and K. Kita, "Molecular interaction in mixed monolayers at the air/water interface," *Adv. Colloid and Interface Sci.*, pp. 1-17, 1999.
- [18] T.D. Gurkov, S.C. Russev, K.D. Danov, I.B. Ivanov, and B. Campbell, "Monolayers of globular proteins on the air/water interface: applicability of the Volmer equation of state," *Langmuir*, pp. 7362-7369, 2003.
- [19] M. Volmer, "Thermodynamic deductions from the equation of state for adsorbed material," *Z. physik. Chem.*, pp. 253-260, 1925.
- [20] I. Langmuir, "Oil lenses on water and the nature of monomolecular expanded films," *J. Chem. Physics*, pp. 756-776, 1933.
- [21] J. He, et al., "Self-Assembly of Tobacco Mosaic Virus at Oil/Water Interfaces," *Langmuir*, pp. 4979-4987, 2009.
- [22] D.W. Britt, J. Buijs, and V. Hlady, "Tobacco mosaic virus adsorption on self-assembled and Langmuir-Blodgett monolayers studied by TIRF and SFM," *Thin Solid Films*, pp. 327-329 and 824-828, 1998.
- [23] T. Rasing, Y.R. Shen, M.W. Kim, and S. Grubb, "Observation of Molecular-Reorientation at a 2-Dimensional-Liquid Phase-Transition" *Phys. Rev. Lett.*, pp. 2903-2906, 1985.

- [24] S.G. Grubb, M.W. Kim, T. Rasing, and Y.R. Shen, "Orientation of molecular monolayers at the liquid liquid interface as studied by optical 2nd harmonic-generation," *Langmuir*, pp. 452-454, 1988.
- [25] L. Gervais, et al., "Immobilization of biotinylated bacteriophages on biosensor surfaces. *Sensor. Actuator. B Chem.*, pages 615-621, 2007.
- [26] D.E. Bradley, and D. Kay, "The fine structure of bacteriophage," *J. Gen. Microbiol.*, pp. 553-563, 1960.
- [27] D.T. Brown, B.T. Burlingh, and N.C. Brown, "Morphology and physical properties of *Staphylococcus* bacteriophage," *J. Virol.*, pp. 664-671, 1972.
- [28] P.J. Rees, and B.A. Fry, "The morphology of staphyococcal bacteriophage-K and DNA metabolism in infected *Staphylococcus aureus*," *J. Gen. Virol.*, pp. 293-307, 1981.